JOURNAL OF THERMOPHYSICS AND HEAT TRANSFER
Vol. 14, No. 4, October–December 2000

Thermal Behavior of Porous Plates Subjected to Air Blowing

Jérôme Bellettre,* Françoise Bataille,† Jean-Claude Rodet,* and André Lallemand‡
Institut National des Sciences Appliquées de Lyon, 69621 Villeurbanne CEDEX, France

The cooling of porous plates by air blowing is studied experimentally. The influences of the air injection rate, of the hot main flow temperature, and of the internal heat exchange surfaces of porous media are determined. The experiments show high efficiency for this cooling process, about 97%. Because of the radiative heat transfer occuring within the test section, a large injection rate (about 5%) is required to reach such an efficiency. The critical injection rate is highlighted. Beyond that value the convective heat transfer does not exist any more because the boundary layer is blown off. Our heat transfer model of the porous plate and its vicinity (convective and radiative transfer) emphasizes important temperature gaps between the solid phase and the fluid phase of the porous media. Fitting the model with the experimental data permits an estimate of the internal heat transfer coefficients.

Nomenclature

c_p	=	specific heat, J/(kg K)
d	=	mean pore diameter, m
F	=	injection rate, $F = (\rho v)_{\text{inj}}/(\rho u)_e$
F_{ij}	=	form factor between walls i and j
h	=	convective heat transfer coefficient, W/(m^2 K) or W/(m^3 K)
J	=	radiosity, W/m^2
Nu	=	Nusselt number, $Nu = h_{\text{int}} d/s\lambda_f$
Pr	=	Prandtl number, $Pr = \mu c_p/\lambda$
q	=	net radiative exchanged heat, W
Re	=	Reynolds number, $Re = \rho v d/\mu$
S	=	surface, m^2
s	=	specific surface, m^2/m^3
T	=	temperature, K
u	=	main flow velocity, m/s
V	=	porous media volume, m^3
v	=	mean velocity of air injected through the porous wall, m/s
x	=	spatial coordinate, m
ε	=	emissivity
λ	=	thermal conductivity, W/(m K)
μ	=	dynamic viscosity, kg/(m s)
ρ	=	density, kg/m^3
σ	=	Stefan–Boltzmann constant, W/(m^2 K^4)
τ	=	transmissivity
Φ	=	exchanged heat, W
φ	=	porosity

Subscripts

conv	=	convective
e	=	potential main flow
f	=	fluid
inj	=	injected or secondary flow
int	=	internal
rad	=	radiometer
s	=	solid phase
sf	=	solid-fluid
w	=	upper surface of the porous wall
wn	=	porous wall normal direction
1	=	longitudinal direction
2	=	vertical direction

Received 22 March 1999; revision received 10 January 2000; accepted for publication 15 January 2000.

*Research Assistant, UMR 5008, Centre de Thermique de Lyon, 20 av. Albert Einstein.

†Associate Professor, UMR 5008, Centre de Thermique de Lyon, 20 av. Albert Einstein; bataille@cethil. insa-lyon.fr.

‡Professor, UMR 5008, Centre de Thermique de Lyon, 20 av. Albert Einstein; a.lal@cethil.insa-lyon.fr.

Introduction

BLOWING is used to protect a solid wall from the detrimental effect of a hot flow (main flow). The wall is made of a porous material, and a coolant (secondary flow) is injected through the wall from the opposite side of the main flow. Thermal protection is caused by both internal cooling and an increase of the boundary-layer thickness, created by the secondary flow on the main flow side. Blowing has met wide acceptance in several applications, especially for rocket engines and turbojets, in drying processes and in the aerodynamics (boundary-layer control). The advantages of this cooling process compared with others such as film cooling are greater efficiency and reduced weight thanks to the use of porous materials.

Blowing has generally been treated by considering either the heat transfer within the porous materials[1–4] or the transfer in boundary layers with blowing.[5–9] To our knowledge, few studies have treated both aspects together: Eckert and Cho[10] and Campolina França et al.[11] on one hand and Kubota[12] and Ishii and Kubota[13] on the other hand.

Eckert and Cho[10] link a low-Reynolds-number k–ε model to a thermal balance within the porous plate; however, the assumption of thermal equilibrium between the gaseous phase and the solid one is required, and radiation toward the plate is neglected. Campolina França et al.[11] study the coupling of a turbulent boundary layer submitted to blowing with a medium equivalent to the porous wall. Both of the earlier approximations, regarding the thermal equilibrium and the radiation, are also made.

Kubota[12] and Ishii and Kubota[13] examine the thermal behavior of a porous matrix, entering the Saturnian atmosphere and cooled by CO_2 blowing. They consider the radiative exchange between the material and its surroundings and the thermal internal nonequilibrium between the gas and the solid. On the other hand, the main flow is not studied, and the convective incident heat transfer is determined by using an attenuation factor caused by blowing. This factor is either constant, whatever the injection rate is, or calculated by using an analytical film model, which corresponds to a first approximation.[14]

It seems worthwhile to link our study of transfer in boundary layers[15,16] to the one of internal transfer within the porous matrix in order to determine the influence of blowing on the solid phase temperature. The porous matrix temperature will be measured in several configurations, using a wind tunnel. The geometry is bidimensional and planar. The wall temperatures of the plate can be calculated using on one hand a model of heat transfer within the porous plate and on the other hand a model of transfer within boundary layers[15,16]

adding the incident radiation toward the plate. The internal heat transfer coefficients are estimated by matching the measured and the calculated temperatures.

Experimental Apparatus

A comprehensive description of the heated wind tunnel is available in Rodet et al.[17]. Its main components are schematically shown in Fig. 1: a 120-kW electrical heater, a 3-m^3/s centrifugal fan, a screen box to reduce the mainstream velocity fluctuations, and a nozzle that delivers air to a test section 0.2 m high, 0.5 m wide, and 2 m long. The test section consists of fixed Pyrex side walls and modular duralumin roof and floor.

A $500 \times 200 \times 3$ mm^3 porous plate is embedded in the floor at 0.865 m from the upstream floor start; the plate is made of sintered stainless steel. Three plates of different types have been used. The type is defined by the internal geometric features, which are the metallic particle mean diameter, the pore mean diameter, and the specific exchange surface. Table 1 summarizes all of these features.

The blowing system delivers air through a 150-mm-high plenum fitted under the porous plate and designed to provide uniform blowing (Fig. 2). The injection rate F varies from 0 to 10%. The relative accuracy of the injection rate measurement depends on two parameters: the coolant flow rate and the class of the plate. This uncertainty is essentially caused by fluctuation of pressure in the injection plenum (around 20 Pa). So, a large coolant mass flow rate will induce an accurate measurement for F. Moreover, the pressure inside the plenum is much lower for class 20 porous plate than for class 10 or 5 plates. Finally, the relative inaccuracy of the injection rate varies between 6.5% (for the lowest F) and 2% (for F reaching 10%) in the case of class 5 and 10 porous plate. In the case of the class 20 plate, the accuracy is less satisfying, and relative errors can reach 9.5% for low injection rates and 3% for the largest F. Consequently, most of the study is performed with class 5 and 10 porous plate. Nevertheless, the class 20 plate is tested, and results concerning this plate should be carefully interpreted, especially for lowest injection rates (less than 1%).

Table 1 Porous plates features

Type	Mean diameter, μm: Metallic particles	Mean diameter, μm: Pores	Specific surface, m^2/m^3
Class 5	50	18	2375 ± 375
Class 10	100	30	1250 ± 250
Class 20	200	75	750 ± 150

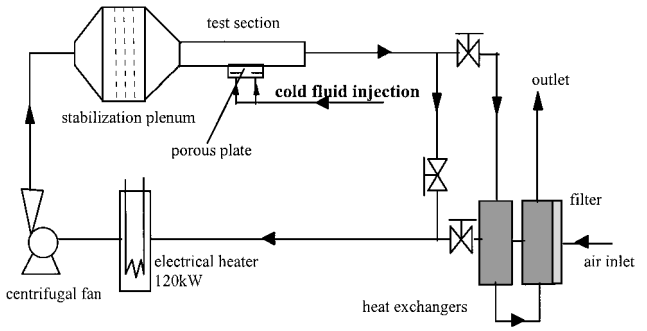

Fig. 1 Heated wind-tunnel setup.

The aerodynamic and thermal features of the bidimensional turbulent boundary layer that is developed on the floor of the test section, in isothermal and nonisothermal conditions, with and without injection and for a given main airflow velocity (10 m/s), have been determined in a previous study.[17] The same configuration will be used in the present paper.

Three windows for infrared (IR) measurements of the porous plate upper surface temperature are fitted within the test section roof. An IR radiometer, moveable from one window to another, can record thermal images of porous plate parts.

Wall Temperature Measurement Methods

A nonintrusive method based on IR thermography was developed to measure the porous plate wall temperature field. It prevents some blocking of the secondary flow in the porous plate and any disturbance to the main flow.

Measurement with an IR Radiometer

Considering 1) the walls within the test section are opaque (Pyrex for the lateral walls, which is opaque in the IR wavelength range, aluminum for the roof and the floor, and sintered stainless steel for the porous plate), 2) the transparency of air for IR radiation, 3) the diffuse and gray behavior of the surfaces, 4) the uniformity of the surface temperatures, so that they can be characterized by a uniform radiosity J_i, the net radiative heat q_i for the surface S_i is

$$q_i = S_i[\varepsilon_i/(1-\varepsilon_i)]\left(\sigma T_i^4 - J_i\right) \tag{1}$$

with

$$J_i = \varepsilon_i \sigma T_i^4 + (1-\varepsilon_i)\sum_{j=1}^{n} J_j F_{ij}$$

The radiative heat received by the radiometer, located above the test section (Fig. 2), from the porous plate is

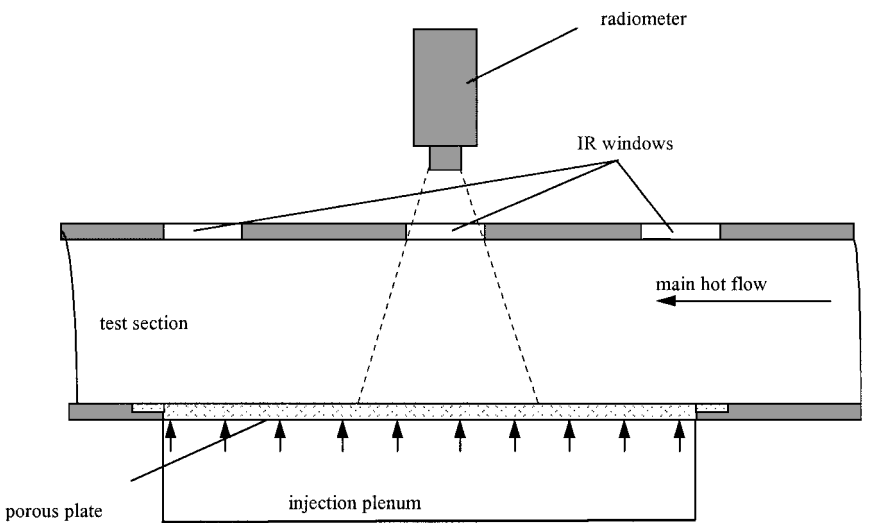

Fig. 2 Measurement configuration within the test section.

$$\Phi_{\text{rad}} = S_w \left[\varepsilon_{\text{wn}} \sigma T_w^4 + \sum_j (1 - \varepsilon_{\text{wn}}) F_{\text{wj}} J_j \right] \tau \qquad (1\text{bis})$$

where τ is the transmissivity of the IR window ($\tau \approx 1$) and F_{wj} is the form factor between the porous plate and the wall j in the test section. The porous plate reflects this radiation toward the radiometer with a reflectivity equal to $1 - \varepsilon_{\text{wn}}$ because its transmissivity equals 0. The normal emissivity ε_{wn} has been determined by Lopes et al.[18] and is equal to 0.85 in the radiometer wavelength range 2.5–5 μm with the temperature range 20–220°C for the class 10 plate. The first term within the brackets represents the radiation of the porous plate, and the second term represents the different test section wall radiation reflected by the porous plate.

After introducing the emissivity ε_{wn}, the temperature measured by the radiometer will be T_w' such that

$$\Phi_{\text{rad}} / S_w = \varepsilon_{\text{wn}} \sigma [T_w']^4 \qquad (2)$$

The unknown temperature T_w and the measured temperature T_w' can be linked by the factor f defined as

$$\varepsilon_{\text{wn}} \sigma [T_w']^4 = f \varepsilon_{\text{wn}} \sigma T_w^4 \qquad (3)$$

then

$$f = \left[\frac{T_w'}{T_w} \right]^4 = 1 + \frac{\sum_j (1 - \varepsilon_{\text{wn}}) F_{\text{wj}} J_j}{\varepsilon_{\text{wn}} \sigma T_w^4} \quad \text{with} \quad \tau = 1 \qquad (4)$$

When blowing occurs through a porous plate whose emissivity is different from 1 (as with our porous plates), f strongly depends on the temperature difference $T_i - T_w$. The temperature difference varies with the injection rate F and is variable along the porous plate. Unless the porous plate is a black body (f equals 1), it is very difficult to estimate the local factor f. Its influence grows as ε_{wn} is smaller. Moreover, some aspect variations of the porous plate surface can change the value of ε_{wn} over rather large ranges. Therefore, this method was given up for the determination of the actual temperature field. Only qualitative results have been obtained. Thermal images of the porous plate, recorded for several blowing and main flow temperature conditions, show that the temperature field is monodimensional, with only streamwise variablility. Moreover, measurements made with the radiometer and linked with other measurements of the porous plate temperature will permit validation of the heat transfer calculation.

Measurement with Welded Thermocouples

To prevent the secondary flow in the porous plate from being blocked and to limit the influence of the test section wall radiation, very thin thermocouples are welded on the upper surface of the porous plate. They are made of two plaited 0.1-mm-diam wires (one in chromel, the other in alumel). Type K thermocouples can withstand temperatures higher than 250°C, and the accuracy of measurements is ±1 K. Thermal images of the porous plate recorded by the radiometer revealed a monodimensional and nonlinear wall temperature field when blowing occurs. As a result, we have welded eight thermocouples along the longitudinal line. Figure 3 presents

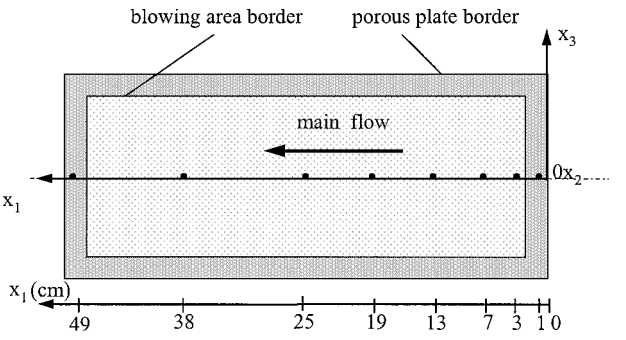

Fig. 3 Thermocouples location on the porous plate.

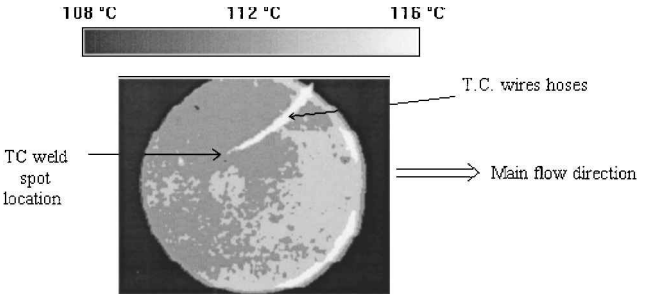

Fig. 4 Thermal image of the porous plate central part with a welded thermocouple.

the locations of the thermocouples along the plate surface. The first and eighth thermocouples are located on the blocked area.

Thermal images of the porous plate recorded for several blowing and main flow temperature conditions show that these thermocouples have no influence on the temperature field. An example is shown in Fig. 4. This thermal image of the porous plate central part, obtained for a main flow temperature of 200°C and an injection rate of 1%, reveals a quasi-uniform temperature field. Except on the boundary of the circular area (perturbation caused by the IR window) and along the thermocouple wires located in the main flow above the porous plate, the wall temperature gradients are at most 4 K. The weld spot does not affect the temperature field.

Experimental Results

Temperature of the Porous Plate

In the first experiment the porous plate class is 10, the velocity of the main flow is equal to 10 m/s, and its temperature is 250°C. The objective is to determine the temperature of the plate at the different locations given by Fig. 3 and to analyze the temperature evolution at different injection rates.

When the plate is not subjected to blowing, its temperature is equal to 224°C. After applying injection, the temperature decreases, as shown in Fig. 5. The temperature of the plate is plotted for injection rates varying from 0 to 10%.

The difference in temperature between the first thermocouple (not submitted to blowing) and the medium thermocouple (the sixth thermocouple) increases with the injection rate until $F = 2.3\%$. Then, at higher injection rates the difference is reduced. At the highest injection rates (around 10%) the plate temperature drops to 34°C. The area located between $x_1 = 19$ and 38 cm is isothermal for all injection rates. Thermal protection is very uniform in this part of the plate.

The difference of temperature, between the first thermocouple and a thermocouple submitted to blowing, reveals a maximum value when F varies. This maximum can be correlated to the critical injection rate, that is, the rate producing the boundary-layer blow off.[19] Plotting the difference of temperature between the first thermocouple and the four following thermocouples as a function of F (Fig. 6) demonstrates that the blowoff starts at the isothermal region of the plate before propagating along the plate. A small increase of the injection rate above the critical rate of the isothermal region (from 2.3 to 2.7%) leads to a blowoff of the whole of the blowing area.

Even when F is greater than the critical rate, the plate temperature always decreases with the injection rate. This is because the plate is only subjected to the radiation of the hot walls of the wind tunnel. The porous plate is only cooled by internal convection assuming that there is a thermal solid-fluid desequilibrium inside the porous medium.

Influence of the Temperature of the Main Flow

To compare the efficiency of the protection process for different temperatures of the main flow, we define the efficiency η by

$$\eta = \frac{T_e - T_w}{T_e - T_{\text{inj}}} \qquad (5)$$

The main flow temperature varies from 100 to 250°C, whereas the injected fluid has a temperature of about 25°C. To calculate the

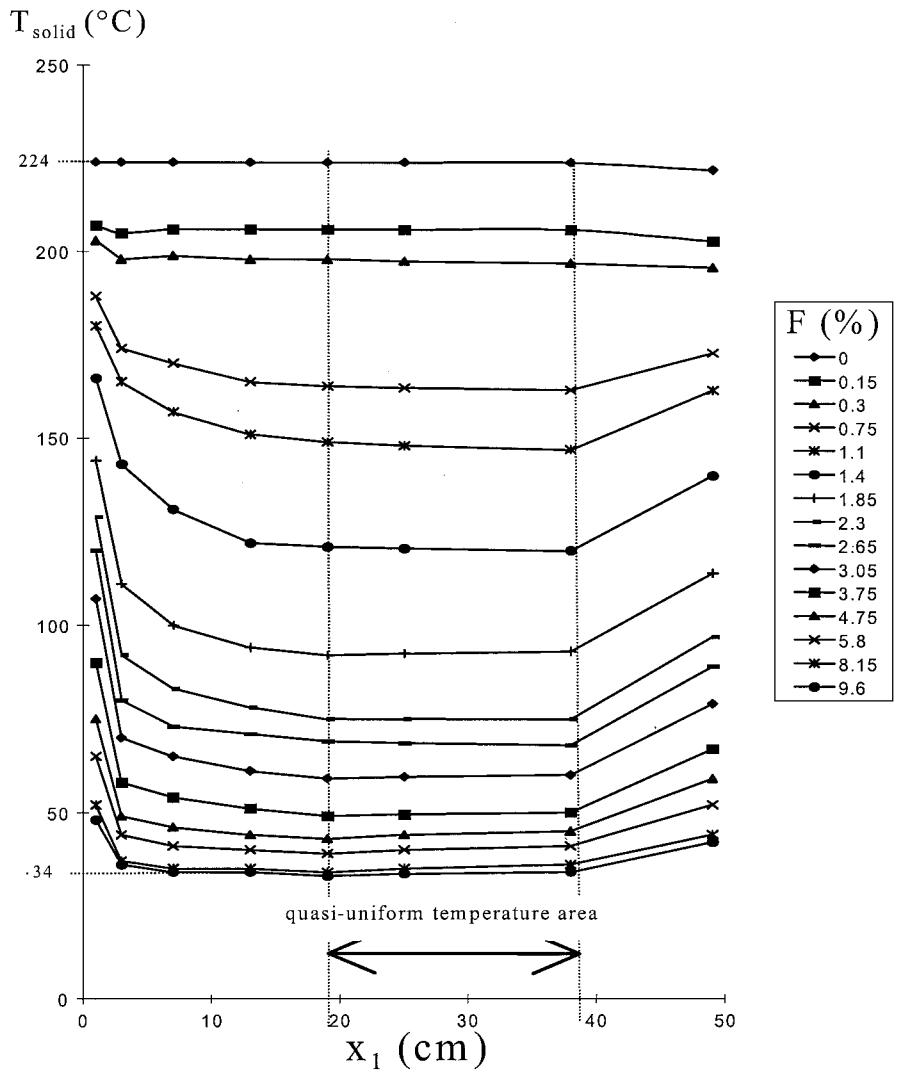

Fig. 5 Wall temperature field for several injection rates (T_e = 250°C, class 10).

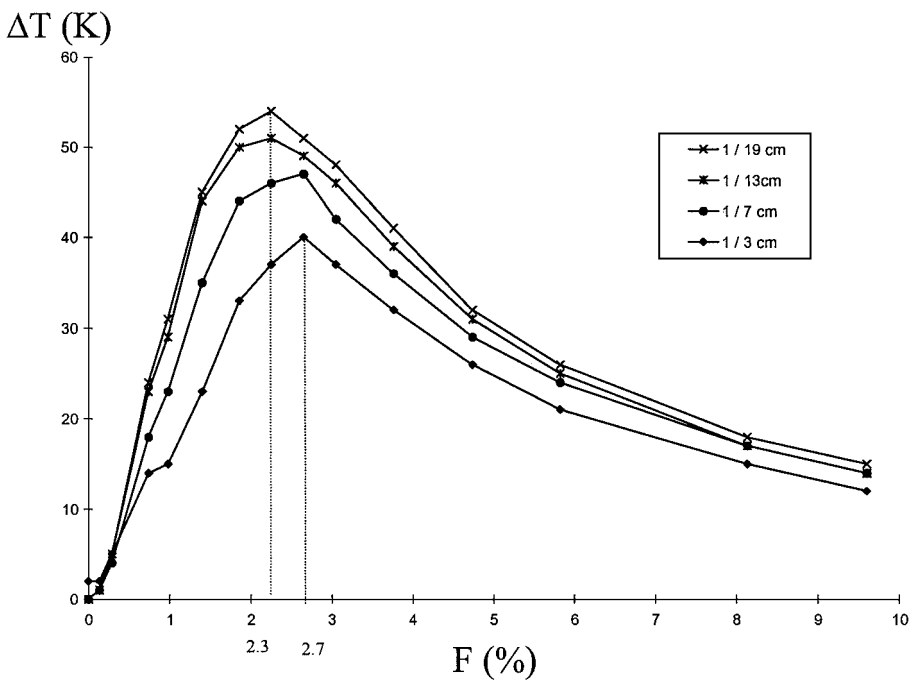

Fig. 6 Temperature differences between the upstream thermocouple and the four subsequent ones vs injection rate.

efficiency, the temperature of the plate is measured at the middle of the porous plate ($x_1 = 25$ cm).

Figure 7 presents the evolution of the efficiency as a function of the injection rate for the different temperatures. All of the curves reach the same level of efficiency (97%) for high injection rates. However, the injection rate to reach this level is larger for higher main flow temperature.

The blowoff of the thermal boundary layer appears for a higher injection rate when the main flow is warmer. This phenomenon can be seen in Fig. 8, where the difference of temperatures, between the first thermocouple and the middle thermocouple ($x_1 = 25$ cm), is plotted as a function of the injection rate for different main flow temperatures. This fact agrees with the results obtained by blowing with different species[8]; the denser the injected gas is (compared to main flow density), the less efficient the blowing effect is. The rates corresponding to the blow off (1.8 to 2.3%) are smaller than the rates corresponding to the efficiency stabilization (3 to 5%). Consequently, the differences observed in Fig. 7 cannot only be explained by the evolution of the critical rate with the temperature. These differences are also caused by the radiation on the plate. For a warmer flow the radiation of the hot walls is more important. To reach the same efficiency, a greater cooling of the plate by internal convection is needed.

Influence of the Porous Media Class

Three different porous media classes are studied for a main flow temperature of 250°C. This temperature corresponds to the case where the exchanged heat fluxes are the largest. The observation has been made that the critical rate is not significantly affected by the class of the porous media at the middle of the plate. In the three cases it remains equal around 2.3% (Ref. 19). Figure 9 shows that the cooling of the porous plate is improved when the size of the pores is small. Furthermore, the difference of temperatures between classes 5 and 10 is larger than that between classes 10 and 20. This must be caused by the evolution of the internal exchange area of the medium, in function of the class. In fact a larger area helps the cooling by internal convection. The difference of specific areas between the classes 5 and 10 is about twice as big as the difference between classes 10 and 20. This trend corresponds to the difference of temperatures that we observed experimentally, although the measurement of class 20 must be analyzed with care because of the important uncertainty for the lowest injection rate. For high injection rates the

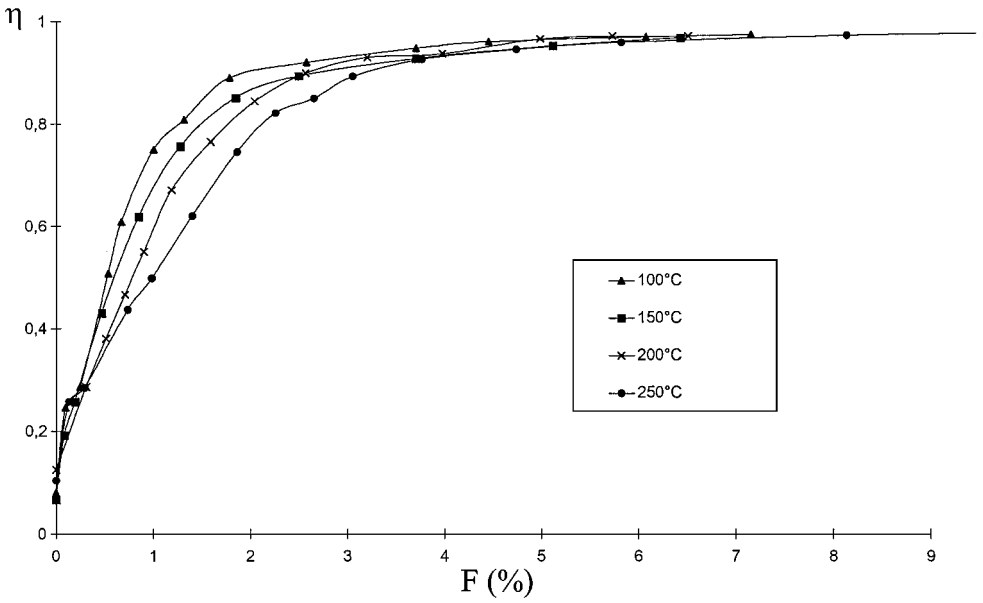

Fig. 7 Cooling efficiency vs injection rate for several main flow temperatures.

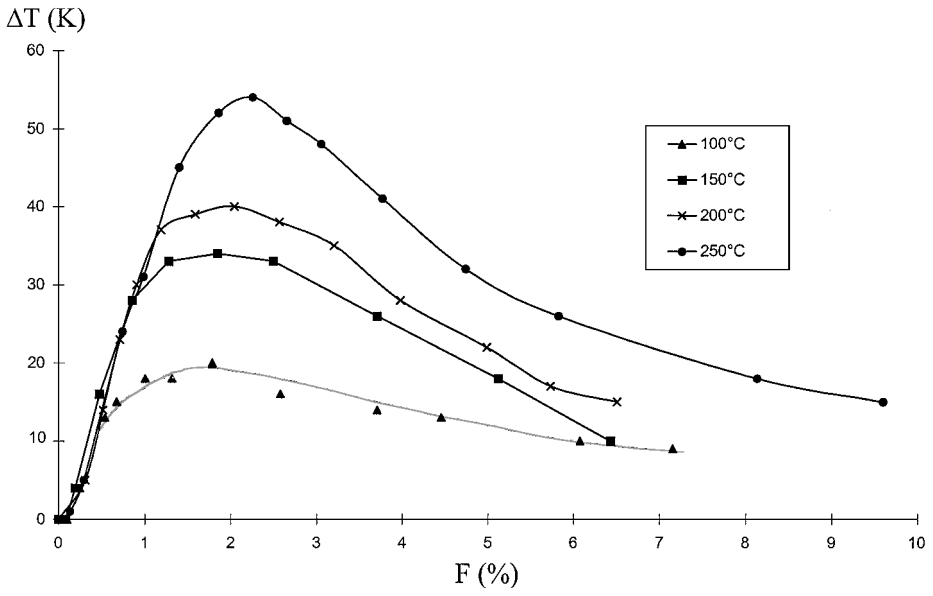

Fig. 8 Temperature difference between the upstream thermocouple and the middle one vs injection rate for several main flow temperatures.

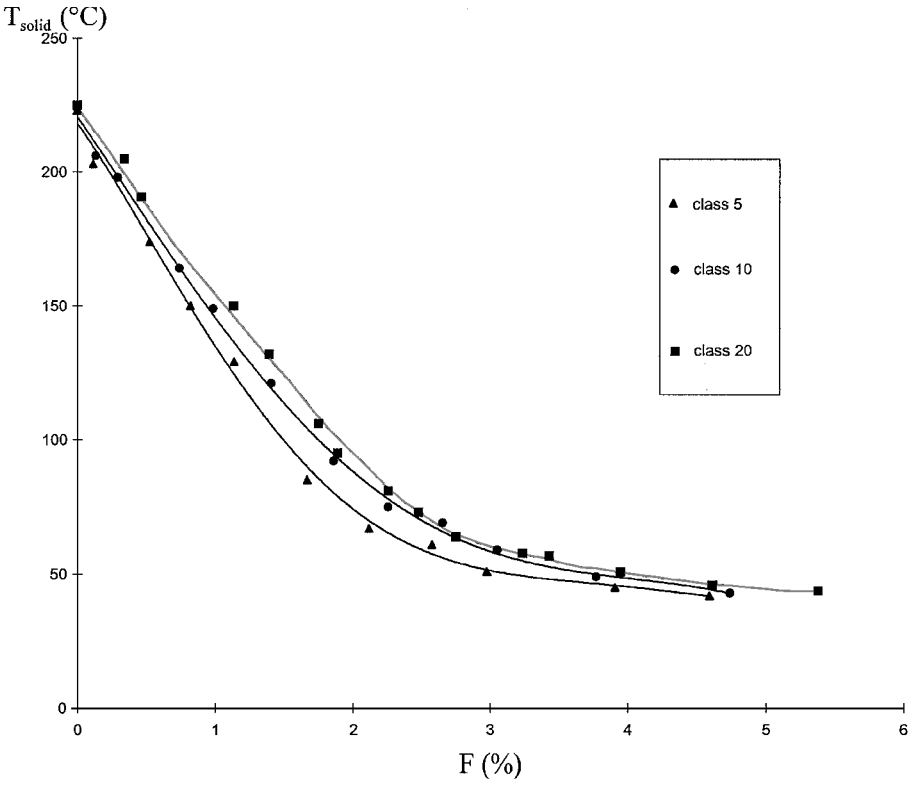

Fig. 9 Temperature at the middle of the porous plate vs injection rate for three different classes.

three curves of temperatures reach the same plateau, corresponding to an efficiency of 97 ± 1%.

The present experimental determination of wall temperatures protected by effusion showed that, for different levels of temperature and for different classes of media, a high efficiency (around 97%) has been obtained. The process of blowing permits excellent protection of the porous walls. Nevertheless, a large injection rate is necessary to get optimal cooling. To quantify the heat transfer between the porous media and its environment, a numerical study is now performed.

Numerical Study of Heat Transfer

Heat transfer inside a porous plate is calculated with the use of two models. The first one is a model of turbulent boundary layers subjected to injection. This first model can predict the convective heat transfer coefficient between the main flow and the porous plate as a function of the injection rate. The main flow is simulated with the finite volume method. The chosen turbulence model is the renormalization group (k–ε) model. Blowing through the porous plate is modeled with a discrete succession of pores and solid particles. Details of this first model can be found in Belletre et al.[15,16] The numerical results of the convective heat transfer on the upper side of a porous plate are used in the second model, which calculates the heat transfer within the porous media. Moreover, the radiation toward the surface of the porous wall is taken into account, using the boundary conditions of this second model. This new model is hereby described in detail and is used to calculate the porous plates temperatures.

Modeling Assumptions

In the modeling of the internal heat transfer, the solid and fluid phases are separated (Fig. 10). Each phase has its own boundary conditions on both sides of the porous wall and the heat exchange between the two phases occurs convectively. The model considers the isothermal region of the porous plate (see experimental data) so that the model domain can be reduced to a simple coupled pore-solid element (Fig. 10). The nodal method is used for the present numerical modeling, and details concerning this numerical method can be found in Bellettre et al.[20]

In the solid element heat transfer is conductive. A thermal contact resistance is introduced between nodes to obtain the equivalent thermal conductivity of the solid matrix (given by Koh and Fortini[21]). Conduction inside the solid particle, in the x_1 direction, is calculated by taking into account the size of the solid element (between 50 and 200 μm). In the fluid phase heat exchange is conductive and convective. The heat flux carried by the fluid movement is calculated with a linear interpolation of the temperature field between two nodes.

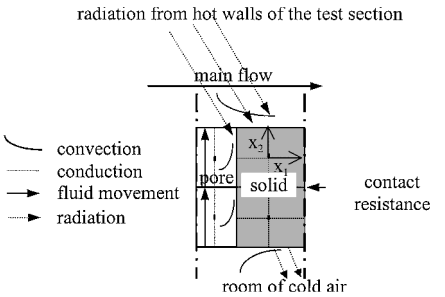

Fig. 10 Heat transfer modeling near and inside the porous wall.

Finally, the heat exchange between the solid and fluid phases is calculated according to relation (6), where h_{int} is the average heat transfer coefficient per unit of porous media volume:

$$\Phi_{\text{conv}} = h_{\text{int}} V \Delta T_{\text{sf}} \tag{6}$$

Boundary conditions on the upper side of porous plates are the following: incident heat fluxes are received only by the solid element of the porous walls. Convective heat transfer coefficient is calculated with the turbulent boundary-layer model[15,16] and the net radiation fluxes by relation (1). The present radiation calculation permits us to take into account the multiple reflexions that occur in our test section. The measured values of hot surface temperatures (lateral glasses and upper side of the wind tunnel) are included in relation (1) so that there is only one unknown (the porous plate temperature) in this relation. On the upper surface of a pore, a convective and radiative heat flux equal to zero is imposed.

Under the porous wall air temperature is imposed (equal to the temperature that is measured 1 mm under the plate). Heat losses of the solid elements toward the injection plenum are the sum of

the radiative heat transfer and convective heat transfer with cold air. (The convective coefficient is calculated with the thermal budget for the porous plate without injection and is supposed not to change with injection.)

Numerical Method

The energy equation is solved for each node in transient state using explicit method. The node temperature at $t + dt$ is calculated as a function of the temperature obtained at time t.

Works concerning heat transfer inside porous media submitted to blowing are numerous.[1–4] However, because of the complexity of the porous media geometry, no universal experimental correlation for the internal heat transfer coefficient h_{int} exists. The internal heat transfer coefficient is then an unknown parameter of this study. Calculated and measured porous plate solid element temperatures are compared, and the internal coefficients are deduced by fitting both temperatures.

Preliminary Results

A possible validation of the radiative heat transfer calculation consists in comparing the porous plate temperatures measured by IR thermography and the calculated temperature. Knowing the real wall temperature (i.e., measured by the thermocouples), it is possible to calculate the radiosity of the plate J_w. Furthermore, the temperature given by the IR radiometer can be estimated by considering that J_w is only the emitted radiation:

$$J_w = \varepsilon_{wn}\sigma T_w^4 + \sum_j (1 - \varepsilon_{wn}) F_{wj} J_j \equiv \varepsilon_{wn}\sigma T_w'^4 \qquad (7)$$

Comparison between the recalculated temperatures T_w' and measurements in the middle of the porous wall is shown on Fig. 11 for a main flow temperature of 200°C. We can see that the gap between thermocouples and IR radiometer measurements is correctly estimated by the present radiation calculation. For high injection rates (when only radiative heat fluxes occur on the porous plate), a discrepancy of 20 K is obtained between measurements by IR radiometer and recalculated temperatures. Otherwise, a 20 K variation of the actual temperature of the porous plate can generate a 15% variation of the porous media net radiative heat flux. This order of magnitude of the accuracy of the radiative heat fluxes calculation is important for the determination of the uncertainty in our final results.

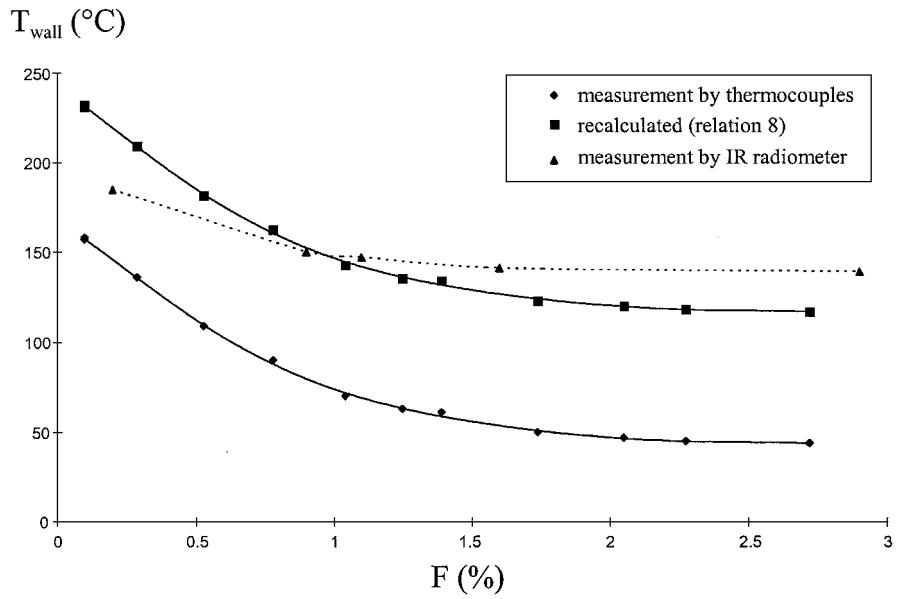

Fig. 11 Wall temperatures measured by thermocouples, by the IR radiometer, and recalculated temperature.

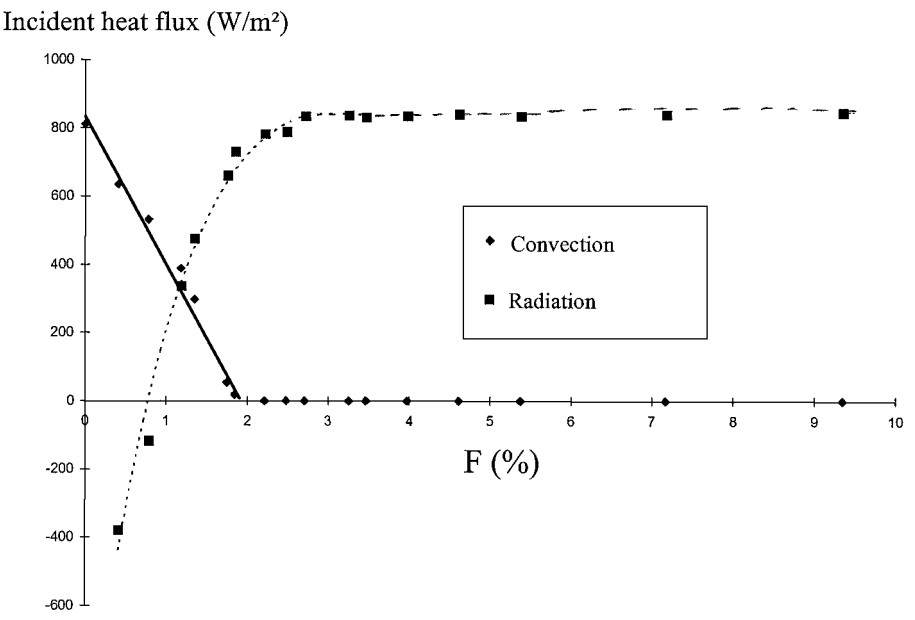

Fig. 12 Convective and radiative incident heat fluxes on the wall (T_e = 250°C, class 20).

Results

Incident heat fluxes on the upper surface of the porous plate are calculated for an injection rate varying from 0 to 10% (Fig. 12). The convective heat transfer between the main flow and the porous wall decreases with the injection rate and reaches a zero value for F around 2%. This injection rate corresponds to the critical injection rate, measured for a 250°C main flow temperature (about 2.3%; see Fig. 8). The radiation received by the wall increases with the decrease of the surface temperature. For low injection rates ($F < 1\%$) the porous wall temperature is higher than those of the other sides of the test section so that the incident radiative flux is negative.

By fitting the calculated and the measured temperatures of the porous-wall solid elements, we calculate the temperature gradients, between both sides of the solid elements, between the inlet and the outlet of a pore, and between the solid and fluid phases. In this way, the convective heat transfer inside the porous media is determined.

We can see a very large temperature gap between the solid phase and the fluid phase in the middle of the porous wall thickness (Fig. 13). By comparison with the calculated vertical temperature gradient (respectively about 3 K for the solid phase and about 20 K for the fluid phase), we can conclude that only a few nodes inside the plate are required for internal heat transfer calculation. These first results were obtained with only two nodes in each phase. A study of sensitivity with the number of nodes (from one to three per phase) shows that the internal temperature gap is modified by only 1 K (Ref. 19). Consequently, the initial number of nodes is kept constant for the following calculations.

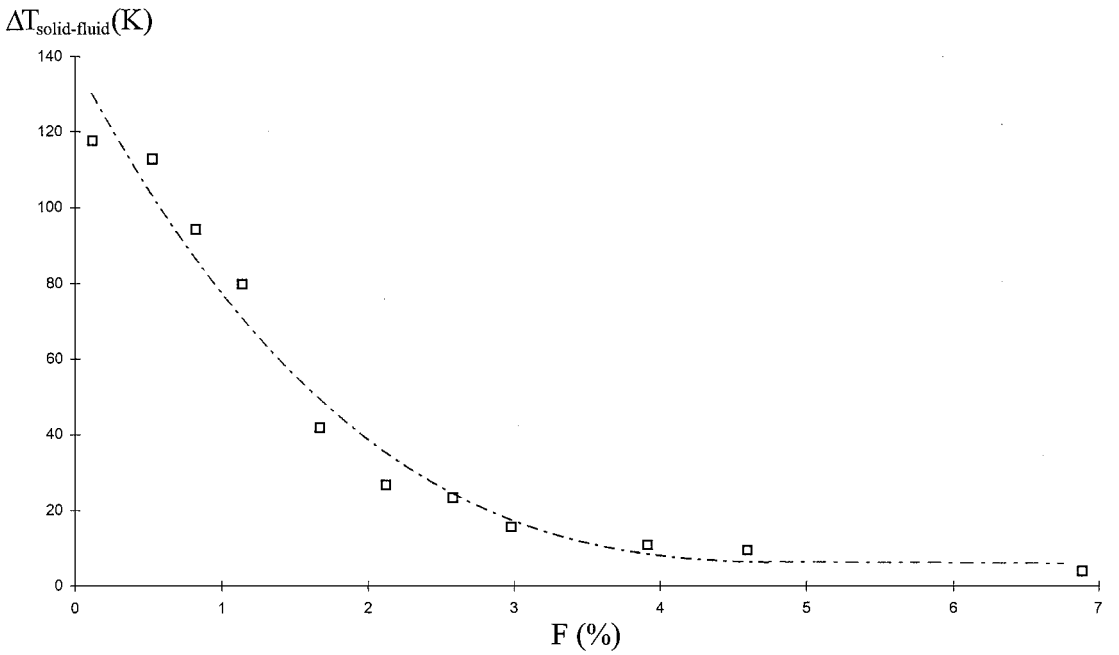

Fig. 13 Internal temperature gap between solid and fluid phases (T_e = 250°C, class 5).

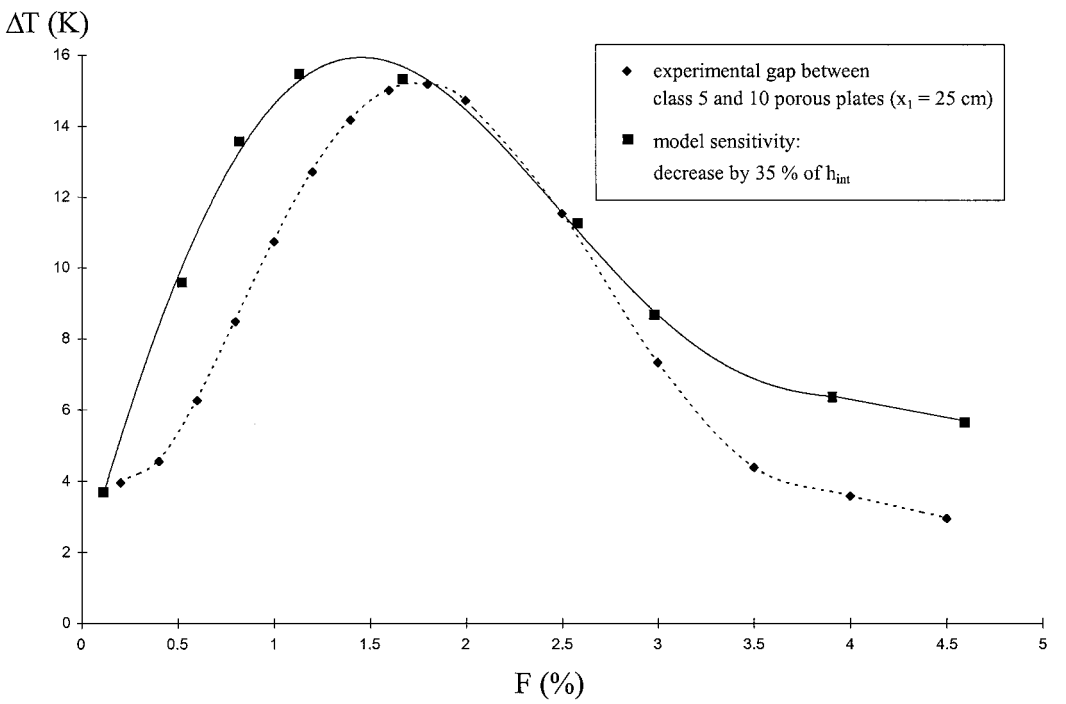

Fig. 14 Effect of the internal heat transfer coefficient decrease on the wall temperature.

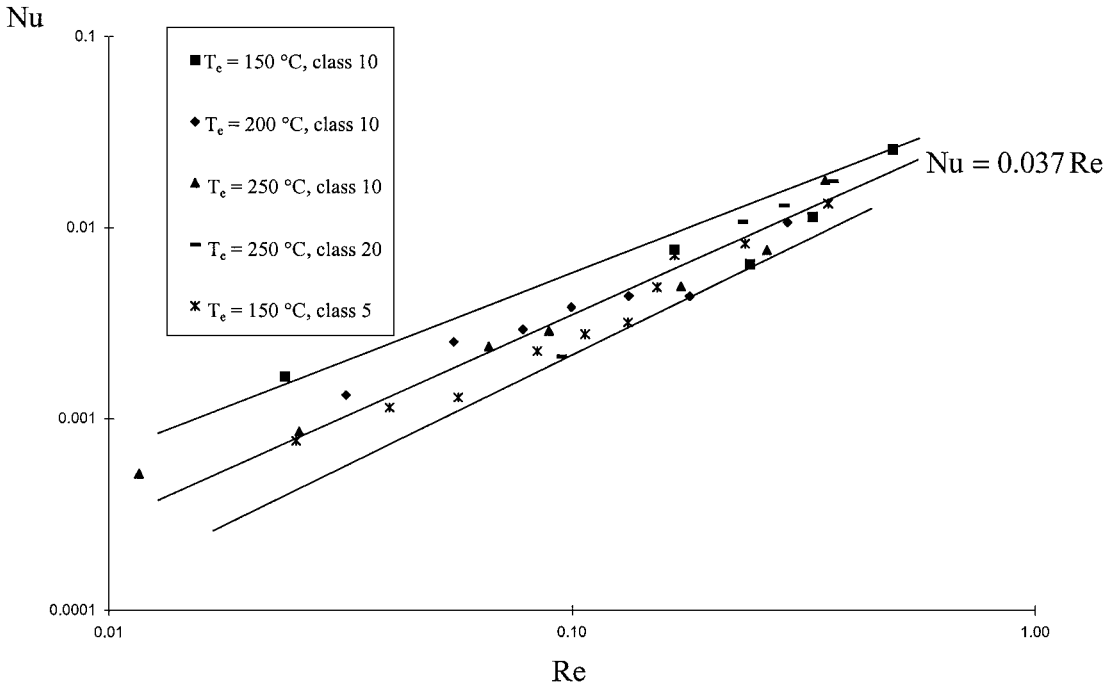

Fig. 15 Nusselt number obtained for rate for different porous plate classes and several main flow temperatures.

Another interesting aspect of this study is the influence of the internal exchange surface of the porous media on the cooling of the plate. Experimentally, a significant gap (its maximum is 15 K) is found between the temperature measured at $x_1 = 25$ cm for class 5 and 10 plates (cf. Fig. 9). The class 10 plate has a smaller internal surface than the one of class 5 (cf. Table 1). Taking into account the uncertainties in specific surfaces, the ratio of the class 5 specific surface over the class 10 one is comprised between 0.36 and 0.75. A sensitivity study is numerically performed in order to see the effect of a decrease of the internal volumetric heat transfer coefficient on the solid element temperature in the case of the class 5 porous plate. The obtained variation of the temperature is similar to the experimental gap as it can be observed in Fig. 14. This result is performed by a decrease of h_{int} by the same order of magnitude (i.e., 35%) than the reduction of the specific surface between class 5 and 10 plates.

Internal heat transfer coefficients are determined for the values of injection rates, main flow temperatures and internal exchange surfaces of porous media, chosen in the experimental part of this study. In Fig. 15 the obtained Nusselt numbers are plotted as a function of Reynolds numbers. The different curves overlap, showing a good modeling of the effects of the main flow temperature and the internal exchange surface of porous media. Using all of the results of the fitting of the model with the experimental data, Nusselt numbers are correlated as a function of Reynolds numbers. The Prandtl number does not vary enough in this study to have a significant effect on Nusselt number. It is integrated as a constant of the correlation. The following correlation is obtained:

$$Nu = 0.037Re \tag{8}$$

The accuracies obtained for the Reynolds number exponent and for the constant value are estimated taking into account all of the uncertainties (injection rate measurement or radiation calculation accuracies). They are respectively 10 and 20%. Our results are close to those of Kar[3] who found a linear variation of the Nusselt number with the Reynolds number for stainless-steel porous media but for Reynolds number a little bit higher than ours: $Nu/Pr^{1/3} = 0.0056Re^{1.06 \pm 0.15}$, for $Re \geq 0.8$.

Conclusions

Sintered-stainless-sted porous plate cooling by injection has been studied experimentally. The effects of the injection rate, of the main flow temperature, and of the porous media specific surfaces have been observed. Wall temperatures have been measured by thermocouples. Infrared thermography has been used to estimate the importance of the radiation and of the multiple reflexions within the test section. The experiments have shown a high efficiency of this cooling process (about 97%). Because of the radiative heat transfer, a large injection rate (about 5%) is required to reach such an efficiency. The results of the heat transfer modeling, inside the porous plate and in its vicinity, have shown that a large temperature gap occurs between the fluid phase and the solid phase. The fitting of the model with the experimental data permitted us to obtain numerous values of internal heat transfer coefficients. Finally, a correlation linking Nusselt numbers to Reynolds numbers is obtained.

To improve the thermal protection of walls, different means are possible. We could increase the internal cooling by choosing porous media with higher internal exchange surfaces. It is also possible to use an absorbing gas as coolant (CO_2 for example) to reduce the incident radiative heat flux. However, a good choice is liquid transpiration because heat quantity absorbed by liquid vaporization is generally very high.

References

[1] Grootenhuis, P., Mackworth, R. C. A., and Sanders, O. A., "Heat Transfer to Air Passing Through Heated Porous Metals," *Proceedings of the General Discussion on Heat Transfer*, Inst. of Mechanical Engineers, London, 1951, pp. 363–366.

[2] Koh, J. C. Y, Dutton, J. L., and Benson, B. A., "Fundamental Study of Transpiration Cooling," Final Rept., NASA CR-134523, Aug. 1973.

[3] Kar, K., "Heat and Mass Transfer Characteristics of the Transpiration Cooling," Dept. of Mechanical and Aerospace Engineering, Ph.D. Dissertation, Case Western Reserve Univ., Cleveland, OH, Sept. 1980.

[4] Yamamoto, S., "Effect of Porosity in Transpiration Cooling System," *17th International Symposium on Space Technology and Sciences*, Vol. 2, 1990, pp. 2355–2360.

[5] Mickley, H. S., Ross, R. C., Squyers, L. C., and Steward, A. L., "Heat, Mass and Momentum Transfer for Flow Over a Flat Plate with Blowing or Suction," NACA TN 3208, July 1954.

[6] Moffat, R. J., and Kays, W. M., "The Turbulent Boundary Layer on a Porous Plate: Experimental Heat Transfer with Uniform Blowing and Suction," *International Journal of Heat and Mass Transfer*, Vol. 11, No. 10, 3208, July 1968, pp. 1547–1566.

[7] Simpson, R. L., "Characteristics of Turbulent Boundary Layers at Low Reynolds Numbers with and Without Transpiration," *Journal of Fluid Mechanics*, Vol. 42, Pt. 4, 1970, pp. 769–802.

[8]Baker, R. J., and Launder, B. E., "The Turbulent Boundary Layer with Foreign Gas Injection. Measurements in Zero Pressure Gradient," *International Journal of Heat and Mass Transfer*, Vol. 17, No. 2, 1974, pp. 275–291.

[9]Silva Freire, A. P., Cruz, D. O. A., and Pellegrini, C. C., "Velocity and Temperature Distributions in Compressible Turbulent Boundary Layers with Heat and Mass Transfer," *International Journal of Heat and Mass Transfer*, Vol. 38, No. 13, 1995, pp. 2507–2515.

[10]Eckert, E. R. G., and Cho, H. H., "Transition from Transpiration to Film Cooling," *International Journal of Heat and Mass Transfer*, Vol. 37, No. 1, 1994, pp. 3–8.

[11]Campolina Franca, G. A., Pagnier, P., and Lallemand, A., "Simulation des Transferts de Masse et de Chaleur par Modélisation à bas Nombres de Reynolds Dans un Écoulement Avec Effusion Locale en Canalisation," *Revue Générale de Thermique*, Vol. 37, No. 3, 1998, pp. 205–222.

[12]Kubota, H., "Thermal Response of a Transpiration-Cooled System in a Radiative and Convective Environment," *Journal of Heat Transfer*, Vol. 99, No. 4, 1977, pp. 628–633.

[13]Ishii, I., and Kubota, H., "Two-Dimensional Response of a Transpiration-Cooled System in a Radiative/Convective Environnement," *AIAA Journal*, Vol. 22, No. 6, 1984, pp. 831–836.

[14]Tedeschi, G., Campolina Franca, G. A., and Lallemand, A., "Refroidissement de Parois Planes par Transpiration: Comparaison de Différents Modèles pour le Calcul des Échanges de Chaleur," *Congrès Français de Thermique*, Elsevier, Paris, 1995, pp. 206–211.

[15]Bellettre, J., Bataille, F., and Lallemand, A., "Study of a Turbulent Boundary Layer with Injection," *1997 ASME Fluids Engineering Division Summer Meeting, Symposium on Separated and Complex Flows* [CD-ROM] 1997.

[16]Bellettre, J., Bataille, F., and Lallemand, A., "A New Approach for the Study of the Turbulent Boundary Layers with Blowing," *International Journal of Heat and Mass Transfer*, Vol. 42, No. 15, 1999, pp. 2905–2920.

[17]Rodet, J. C., Campolina Franca, G. A., Pagnier, P., Morel, R., and Lallemand, A., "Etude en Soufflerie Thermique du Refroidissement de Parois Poreuses par Effusion de Gaz," *Revue Générale de Thermique*, Vol. 37, No. 2, 1998, pp. 123–136.

[18]Lopes, R., Moura, L. M., Baillis, D., and Sacadura, J. F., "Directional Spectral Emissivity of a Packed Bed: Correlation of Theoretical Prediction and Experimental Data," *IMCE, American Society of Mechanical Engineers. International Mechanical Engineering Congress*, Anaheim, CA, 1998, pp. 157–162.

[19]Bellettre, J., "Transferts de Masse et de Chaleur dans la Couche Limite Pariétale et à l'Intérieur d'une Paroi Poreuse Plane Soumise à de l'Effusion ou de la Transpiration," M.S. Thesis, Energy and Heat Transfer Dept., INSA de Lyon, France, Dec. 1998.

[20]Bellettre, J., Sartre, V., Biais, F., and Lallemand, A., "Transient Study of Electric Motor Heating and Phase Change Solid-Liquid Cooling," *Applied Thermal Engineering*, Vol. 17, No. 1, 1997, pp. 17–31.

[21]Koh, J. C. Y., and Fortini, A., "Prédiction of Thermal Conductivity and Electrical Resistivity of Porous Metallic Materials," *International Journal of Heat and Mass Transfer*, Vol. 16, No. 11, 1993, pp. 2013–2022.